Support vector regression-based grid localization method for acoustic emission sources from Chinese fir boards

GuoFeng Wang
Beijing Forestry University
E-mail: wangguofengbjfu@163.com

*Dong Zhao**
Beijing Forestry University
E-mail: zhaodong68@bjfu.edu.cn

(Received 20 December 2024)

Abstract. Wood is an anisotropic composite material, whose variation can make it difficult to locate surface damage using non-destructive testing. In order to solve the problem of sound source localization on the surface of wood, this study used a first localization method combining grid-based feature mapping and machine learning. Chinese fir boards (*Cunninghamia lanceolata*) were divided into a grid and acoustic emission signals were generated through a pencil-lead break test. These signals were processed using wavelet packet decomposition (WPD) to create a database of energy feature vectors. Localization was then achieved by applying support vector regression (SVR), which compared the feature vectors from the experimental points with those in the database to determine the sound source location. The average absolute error of this localization method was 7.51 mm, the average relative error was 3.79%, and the positioning accuracy was 91.84%, which can effectively locate the sound source on the wood surface.

Keywords: Acoustic emission, Signal processing, Machine learning, Signal prediction, Grid localization

Introduction

The evaluation of wooden members is crucial for the proper functioning of the entire wooden structure (Lamy et al. 2015; Han et al. 2022). Although many methods for structural non-destructive testing (NDT) exist (Nocetti et al. 2023; López et al. 2023; Xu et al. 2023; Guo et al. 2017), few can achieve real-time dynamic assessment (Ji et al. 2023), i.e., structural damage monitoring and localization under normal working conditions. In particular, wood exhibits varying moduli of elasticity in different directions (Dinçkal 2011), which affects sound source localization. Low localization accuracy remains a key challenge for using acoustic emission as a non-destructive testing technology.

Sound source localization refers to the process of determining the origin of acoustic emissions by analyzing the characteristics of sound waves (Qin et al. 2024; Zhou et al. 2023; He and Zhu 2024; Li et al. 2018). In the context of wooden structures, this technique is particularly valuable for detecting damage, such as cracks or voids (Aicher et al. 2001; Pan et al. 2024; Boccacci et al. 2022). It plays a critical role in ensuring the structural integrity and safety of wooden components, especially in applications such as wooden buildings (Rescalvo et al. 2018), furniture (Ai et al. 2024), and cultural heritage preservation (Cruz et al. 2022; Xu et al. 2021). The ability to accurately locate sound sources in wood is essential for real-time structural health monitoring and damage assessment. Despite its potential, the anisotropic nature of wood poses significant challenges to achieving high localization accuracy, which limits the widespread adoption of this technology.

At present, there are two main research methods for sound source localization: signal arrival time-based research and signal processing-based research. In arrival time-based sound source localization, Kundu et al. (2007) used multiple sensors to obtain the arrival time differences of sound source signals and used additional information, such as the angle between the sensors and the sound source, to determine signal location. Yin et al. (2021) improved the relative positioning of the sensors to further enhance the accuracy of the arrival time-based localization method. They also constructed a composite material model through finite element simulation to verify the effectiveness of the proposed method. Park et al. (2012) used four sensors to collect signals, construct arrival time differences, and build a neural network database to predict signal position. However, propagation speed of the stress wave signals in anisotropic

* Corresponding author

materials varies depending on the direction, so it is difficult to accurately detect the arrival time of the signals in each direction, and ultimately making it difficult to determine the exact location of the sound source generation. Therefore, researchers proposed a sound source localization method based on stress wave signal processing. In the research of sound source localization based on stress wave signal processing: Shrestha et al. (2015) constructed a signal database by processing the signals collected by traversing each sound source point, and then determining the location of the sound source by comparing the correlation coefficients; Zhao et al. (2017) proposed a wood energy attenuation model to determine the location of damage to the wood structure; Su et al. (2012) constructed a support vector regression (SVR) model based on acoustic emission signal features for the spatial 3D structural localization of anisotropic materials; Ebrahimkhanlou and Salamone (2018) proposed a method that combined dispersion and modal characteristics of signals with a neural network. In this approach, only a single transducer was used to locate the sound source region. This method effectively overcame the effects of wave velocity attenuation and reduced the number of sensors required. However, the localized object was structurally simple, limiting the method's generalizability.

Since wood is an orthogonal anisotropic material (Bucur 2023), the performance differences were smaller when structural neighboring positions were closer. Therefore, this paper proposes a grid localization method for wood sound sources. This method leverages the fact that as the distance between the acoustic emission source positions decreases, the influence of wood texture diminishes, and the frequency-domain features of the signals received by the sensors become more similar. It employs wavelet packet decomposition (WPD) for energy feature extraction and combines it with SVR to achieve accurate sound source localization. The main process of the research is as follows (Figure 1): ① Divide a limited number of grids into sample points on the wood. Break the lead at these sample points and extract the energy of each frequency band from the signals collected by the acoustic emission sensors using wavelet packet noise reduction and transformation. ② Apply principal component analysis (PCA) for dimensionality reduction to enhance feature vector differentiation, then input the low-dimensional feature vectors into a SVR to build a model. ③ Break the lead at various positions on another board, collect acoustic emission signals, and perform WPD to extract the wavelet packet energy feature vector. ④ Use the SVR to complete the localization of the acoustic emission source. The main advantage of this method is that grid division reduces the influence of wood anisotropy within a local range, and when combined with wavelet packet feature extraction, it further minimizes the impact of wood anisotropy on positioning accuracy. At the same time, using only a single sensor avoids the problems of multi-sensor signal interference and wave velocity attenuation, thereby significantly improving the accuracy and practicality of positioning. This method provides a new

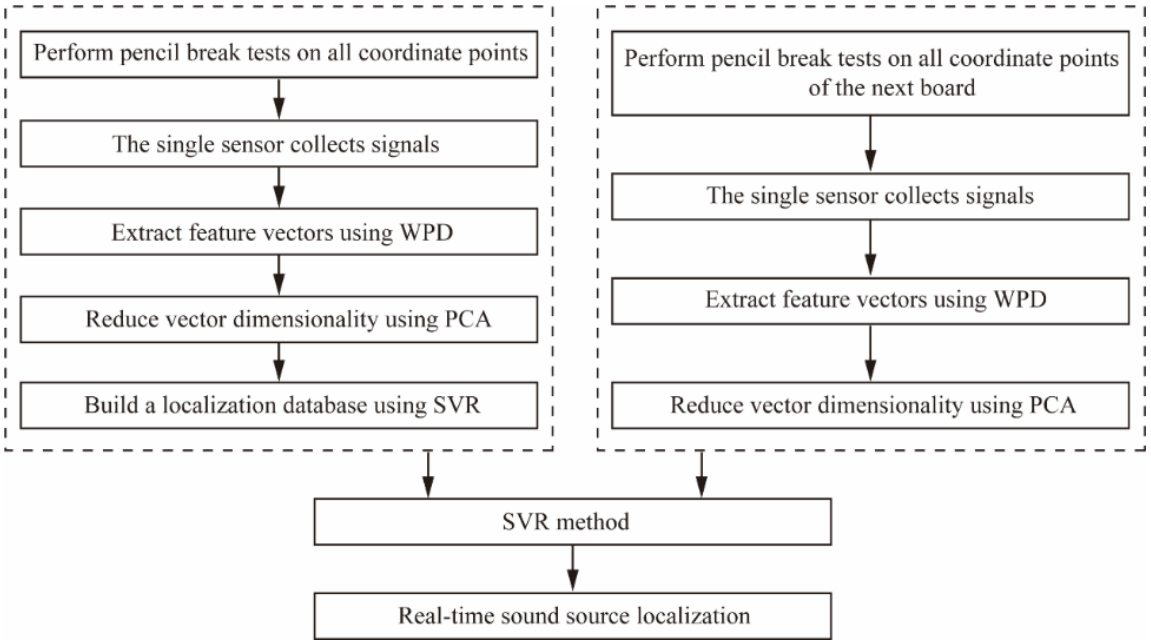

Figure 1. Sound source localization flowchart.

solution for non-destructive testing of wood, with potential applications in real-time structural health monitoring, quality control in wood processing, and cultural heritage preservation.

Material and methods

Test system

The acoustic emission signal acquisition system consisted of a DS2 acoustic emission analyzer, an RS-2A acoustic emission sensor, and a front amplifier with adjustable gain (40 dB, 5 V output). According to the Shannon-Nyquist sampling theorem, the sampling frequency was set to 500 kHz (Li et al. 2020). When the acoustic emission signal propagates in the wood, the value of its energy decreases with increased distance from the source; the distance between the sound source and the acoustic emission sensor was 0–200 mm (Zhao et al. 2017). Therefore, the maximum distance between the transducer and the excitation point should not be more than 200 mm from the surface of the wood. High temperature vacuum grease was used to connect the transducer to the wood sample.

Two rectangular defect-free boards of Chinese fir (*Cunninghamia lanceolata*) from adjacent areas of the same parent board (named "fir board 1" and "fir board 2"). The boards had similar ratios of sapwood and heartwood, and were used to construct the training samples and test samples, respectively. The experiment used a rectangular board with fixed support on all four sides, which measured 185 mm × 140 mm × 20 mm (length × width × thickness) with a density of 0.306 g/cm^3. A 140 mm × 140 mm square was used for the lead-breaking experiments (Figure 2). Taking 7 × 7 grids as an example, the coordinate system was established (Figure 2b), and the planks were aligned with the y-axis and x-axis directions in the down-grain direction and cross-grain direction, respectively.

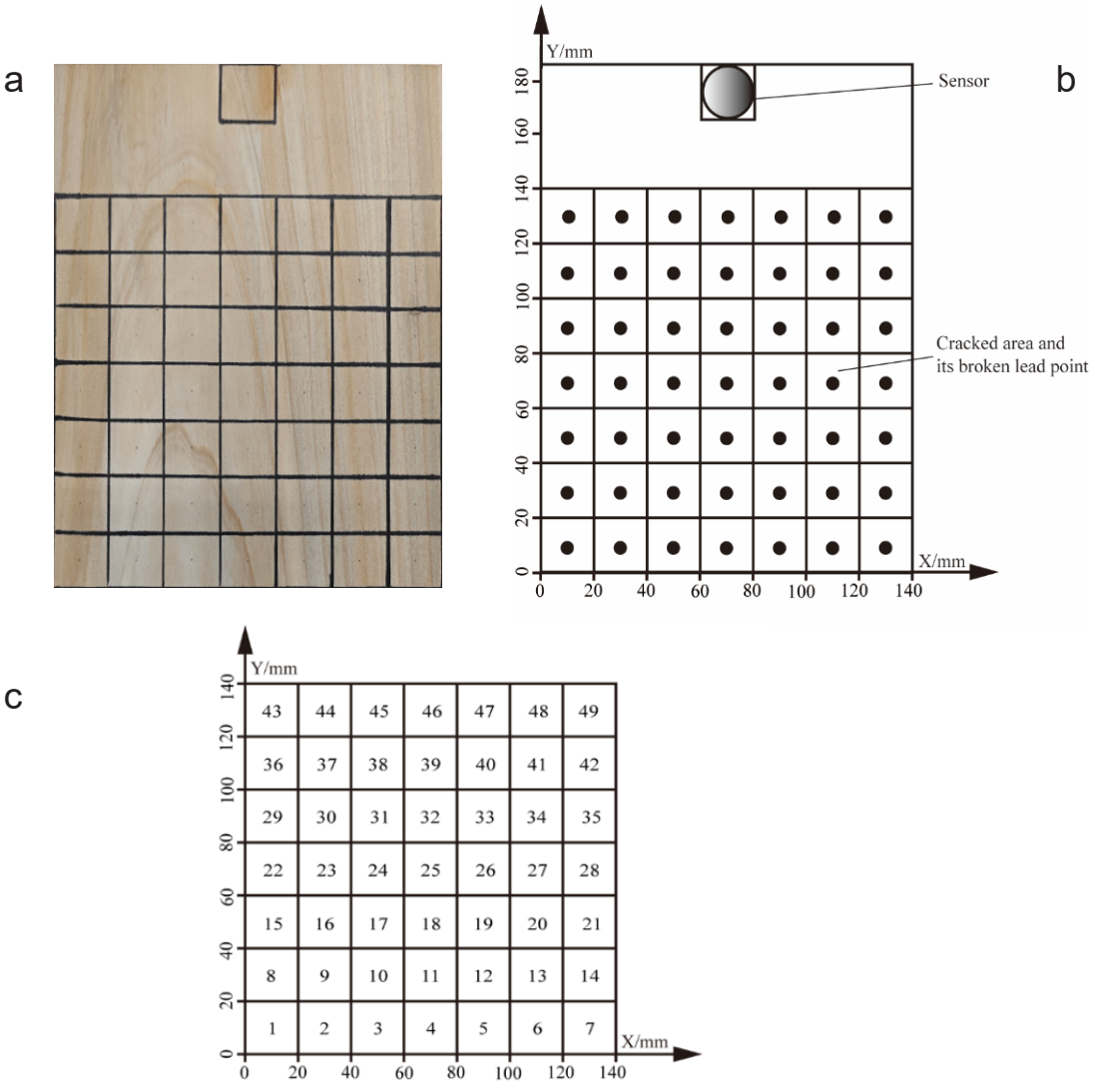

Figure 2. (a) Grid division, (b) sensor layout, and (c) lead breakage point location of fir boards.

In accordance with the ASTM standard (American Society for Testing and Materials), the geometric center of each grid area was broken with a Hsu-Nisisen quill (2H/0.5 mm), and a signal excitation was applied to generate an acoustic source, i.e., the signal generated by the simulated crack. The coordinates of the geometric center point of a single transducer were 70 mm by 175 mm. The minimum distance between the transducer and the signal excitation point was 35 mm, and the maximum distance was 175.57 mm.

Wavelet packet energy feature vector extraction

The wavelet packet method decomposes both high-frequency and low-frequency components of the signal layer by layer until reaching the predetermined decomposition level. A 3-level WPD of the original signal S yielded the signal components S_{3-0}, and S_{3-1} … S_{3-7} (Figure 3).

The Daubechies (db) wavelet has the advantages of orthogonality, tight support, approximate symmetry, and the ability to perform discrete wavelet transform, which can be fully reconstructed. Through layer-wise decomposition, acoustic emission signals yield increasingly detailed wavelet packet energy feature vectors; however, beyond a certain number of layers, the increase in sensitivity to the acoustic emission signal of wood is not obvious. For comprehensive consideration, this paper adopted the db5 wavelet to calculate the energy feature vectors of each frequency band of the wavelet packet in the 9th layer, which was used as the input index of the SVR:

$$[\lambda_1, \lambda_2, \lambda_3, \lambda_4, \lambda_5, \lambda_6, \cdots] \quad (1)$$

For every λ there is:

$$\lambda_j = \frac{E_{9,j}}{\sum_{i=1}^{n} E_{9,j}} \quad (2)$$

Where: $E_{9,j}$ stands for the energy of the 9th component of the 9th layer wavelet packet j. In addition, the energy ratio of the wavelet packet is characterized as:

$$\int_0^{+\infty} \frac{da}{a^2} \int_{-\infty}^{+\infty} |WT_x(a,b)|^2 \, db = C_\Psi \int_{-\infty}^{+\infty} |x(t)|^2 dt \quad (3)$$

$$C_\Psi = \int_{-\infty}^{+\infty} \frac{|\Psi(\omega)|^2}{\omega} d\omega \quad (4)$$

Where: $WT_\chi(a,b)$ is the wavelet packet coefficients; C_ψ is the coefficient that converts the wavelet packet energy to the time domain energy; $\Psi(\omega)$ is the wavelet tolerance condition; ω is the frequency.

The energy of each wavelet packet component is the sum of the squares of the coefficients of that wavelet packet, i.e.:

$$E = \sum (d_i)^2 \quad (5)$$

Where: d_i is the coefficient of the wavelet packet in which it is located.

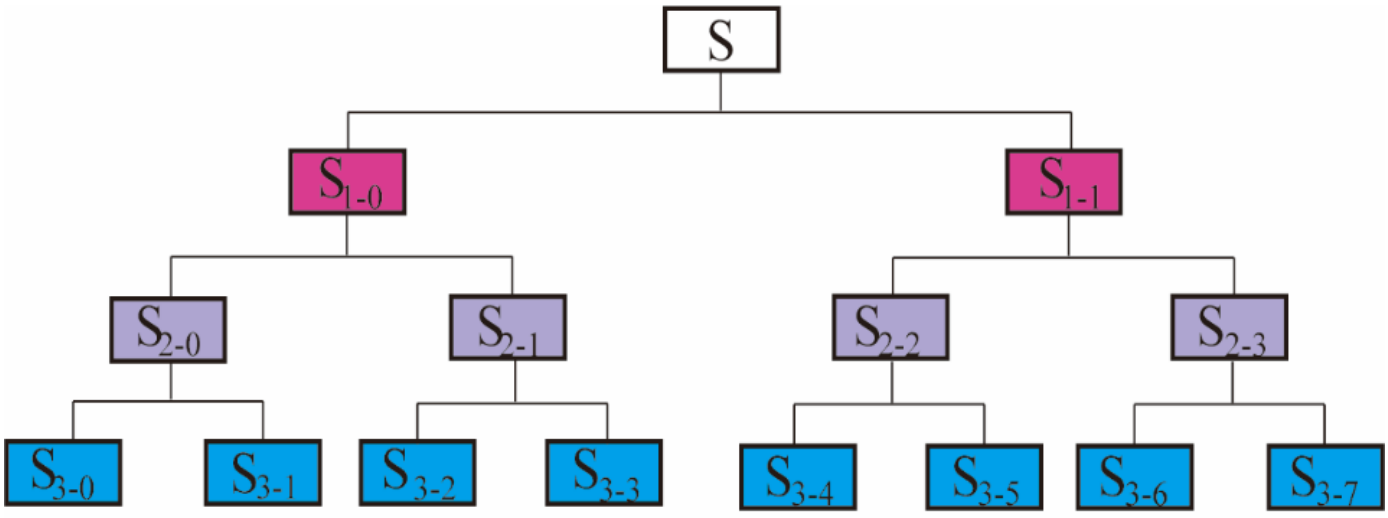

Figure 3. 3-level Wavelet packet decomposition.

So, the wavelet packet energy $E_{9,j}$ can also be expressed as:

$$E_{9,j} = \sum (d_{9,j,i})^2 \quad (6)$$

Where: $d_{9,j,i}$ represents the $S_{9,j}$ coefficient.

Support vector regression principle

Acoustic emission signals were decomposed into energy feature vectors by wavelet packet methods, and the feature dimensions were usually between tens and hundreds, which needed to be reduced to be used as inputs to the localization model. Considering the number of samples and feature dimensions, this paper chose the SVR algorithm to construct the acoustic emission localization model.

The SVR algorithm was a supervised learning algorithm used to predict discrete values. The samples were assumed to be *(x,y)*; *f(x)* was the output; *y* was the desired outcome; ω and *b* were the parameters to be determined; ε was the maximum permissible deviation; the solid and hollow circles denoted the samples with no loss computed and the samples with loss computed (Figure 4). The objective function of SVR is:

$$\min_{\varepsilon,b} \frac{1}{2}||\omega||^2 + C\sum_{i=1}^{m} l_\varepsilon(f(x_i) - y_i) \quad (7)$$

C is the regularization parameter and l_ε is the ε-insensitive loss function:

$$l_\varepsilon(y - f(x)) = \begin{cases} 0, |y - f(x)| \le \varepsilon \\ |y - f(x)| - \varepsilon, \text{else} \end{cases} \quad (8)$$

Introducing the slack variables ξ_i and $\hat{\xi}_i$ yields:

$$\min_{\omega,b,\xi,\hat{\xi}} \frac{1}{2}||\omega||^2 + C\sum_{i=1}^{m}(\xi_i + \hat{\xi}_i) \quad (9)$$

$$\text{s.t. } f(x_i) - y_i \le \varepsilon + \xi_i$$

$$y_i - f(x_i) \le \varepsilon + \hat{\xi}_i$$

The SVR function is obtained according to the KKT condition:

$$f(x) = \sum_{i=1}^{m}(\hat{\alpha}_i - \alpha_i)\kappa(x, x_i) + b \quad (10)$$

Where: $\kappa(x_i, x_j) = \varphi(x_i)^T(x_j)$ is the kernel function.

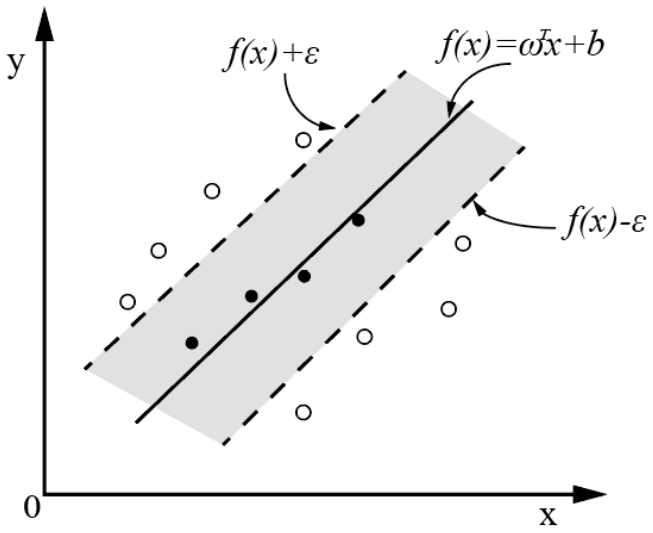

Figure 4. Schematic diagram of support vector regression.

Grid localization method

The principle of SVR method for Chinese fir board sound-source grid localization was as follows: firstly, a suitable SVR model was selected according to the prediction object, and the regression model was trained by training samples. According to the training samples in the delineated grid, a regression function was expressed as

$$f(x) = \sum_{i=1}^{m}(\hat{\alpha}_i - \alpha_i)\kappa(x, x_i) + b$$

The SVR training model based on radial basis kernel function was obtained, at this time, the predicted value of the sample points was determined by the regression function and loss function.

Constructing an energy feature vector localization model

Wavelet packet denoising was implemented using a MATLAB-based signal processing program. The original signal underwent 4-level decomposition using the db5 wavelet, followed by removal of the noise-dominated low-frequency band. The remaining frequency components, free from fundamental frequency interference, were then reconstructed, resulting in a denoised signal with enhanced robustness for source localization. The original acoustic emission signal in grid region 1 was given (Figure 5a), as well as the signal after noise reduction by removing disturbances such as environmental and electromagnetic noise (Figure 5b).

Each signal after the noise reduction process was subjected to a 9-layer WPD of db5 wavelets to obtain a 512-dimensional

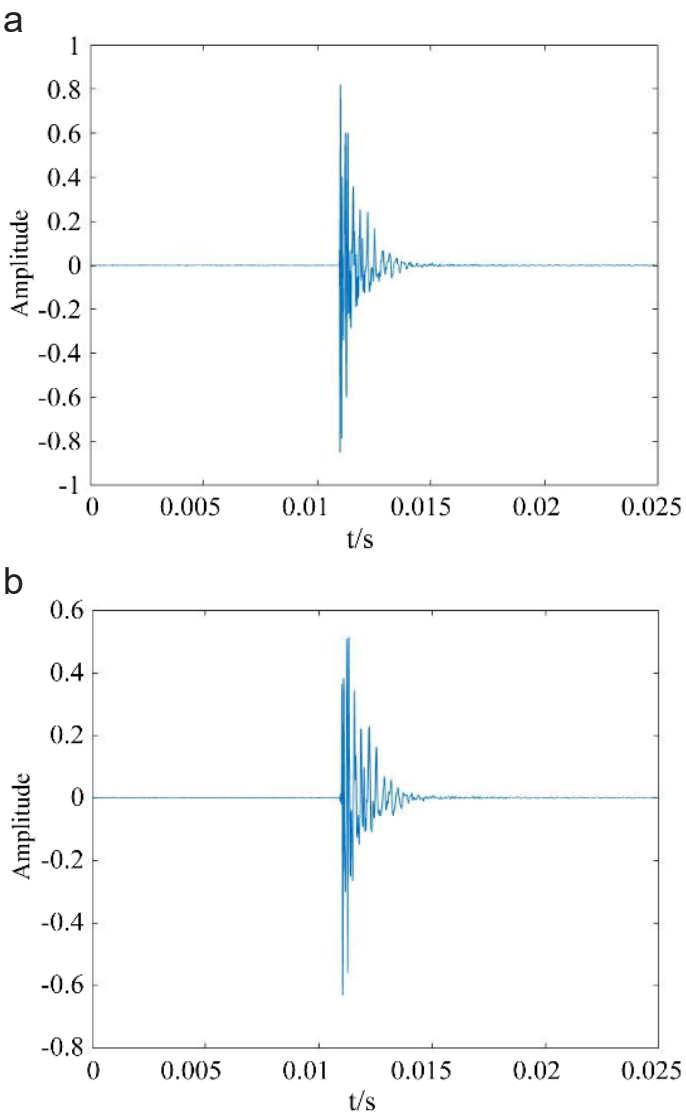

Figure 5. The original signal and denoised signal in grid area 1: (a) Original signal (b) Noise reduction signal.

energy feature vector $[\lambda_1, \lambda_2, \lambda_3, \cdots, \lambda_{512}]$. However, the larger the dimension of the energy feature vector, the more complicated the data calculation when machine learning is performed. This paper utilized the PCA method for dimensionality reduction to obtain the feature vector $[\lambda_1', \lambda_2', \lambda_3', \cdots, \lambda_{244}']$. In this paper, the first 8-dimensional feature vectors with a cumulative contribution rate of more than 99% were selected as the input data for the SVR.

Experimental localization

In order to verify the effectiveness of the SVR method for sound source grid localization on wood boards, localization tests were conducted on thin Chinese fir boards. Forty-nine sample points were used for lead break training on each board, as follows: each sample point on fir board 1 was applied 4 times, for a total of 196 lead breaks to construct the training sample; and each sample point on fir board 2 was applied 1 time, for a total of 49 lead breaks to construct the test sample. This resulted in 245 lead break signals, which constituted the sample matrix $[t_1, t_2, t_3, \cdots, t_{245}]$, where the samples $t_i = [\lambda_1', \lambda_2', \lambda_3', \cdots, \lambda_{244}']_i$. The normalized feature vectors are used to train the SVR model. In the process of SVR modeling, the best penalty coefficient c and kernel function g can be determined by using the cross-validation method, and the final result obtained by the SVR prediction was the localization result. Assuming that the sound source location was l_i, $i = 1, 2 \ldots n$, when using the SVR for sound source localization, the sound source location was expressed as:

$$l = arg \min_{l_i} \frac{2}{\| w \|} \tag{11}$$

Results and discussion

Because of differences in wavelet packet energy amplitude of each sub-band of the acoustic emission signals at different locations, the similarity between the signals at each location differed, and similarity was calculated by the formula (Guo et al. 2017) as:

$$R = \frac{\sum_{i=1}^{n}(x_i - \overline{x})\,(y_i - \overline{y})}{\sqrt{\sum_{i=1}^{n}(x_i - \overline{x})^2 \sum_{i=1}^{n}(y_i - \overline{y})^2}} \tag{12}$$

Where: n is the dimension of the feature vector; $\bar{x}$, and $\bar{y}$ is the mean value of vector x, y. The feature vector of the acoustic emission signal at the coordinates 70 mm, 130 mm in the training set database, i.e., the signal vector of this sample point, was compared with the vector of the acoustic emission signal at each position in the database in terms of similarity. The results (Figure 6) showed that the signal had a high degree of similarity to the feature vector of the nearby signal with a maximum of 1 with this point, and a low degree of similarity to the feature vectors of signals farther away. The signal vector at the coordinates 70 mm, 130 mm was compared with the test signal vectors at each location for similarity (Figure 7) and also showed that the signal had a high degree of similarity with the nearby test signal. The test signal was a maximum of 0.99 at that point, with a low degree of similarity with the more distant test signal. These results suggest that the closer the relative distance between the sound sources, the smaller the difference produced by their signal energy distribution. These results support the premise that the closer the distance

between the locations of the acoustic emission sources, the more similar the frequency domain characteristics of the signal received by the sensor. These results suggest that machine learning methods can be used to train the sound source location using the differences in vectors of wood panels in different grid regions to recognize and evaluate the acoustic emission source location of wood.

The dimension-reduced feature vectors of training samples were used to train an SVR-based sound source localization model that predicted both the coordinates and grid regions of test samples (Figures 8a and 8b). The prediction errors were quantified using the following metrics:

$$S = \sqrt{(x - x_0)^2 + (y - y_0)^2} \tag{13}$$

$$P = \frac{\sqrt{(x - x_0)^2 + (y - y_0)^2}}{140\sqrt{2}} \times 100\% \tag{14}$$

where: s denotes absolute error; p denotes relative error; x, y denotes the position coordinates of the center point of the predicted grid region in x- and y-directions, respectively; x_0, y_0 denotes the position coordinates of the x- and y-directions of the center point of the predetermined grid region, respectively.

Taking the sound source grid size of 20 mm × 20 mm as an example, the sound source localization resolution was 20 mm, and the pencil-lead break test was performed sequentially at 49 positions on the fir board. The average absolute error of the predicted values for all grid areas was 7.51 mm, with an average relative error of 3.79%. Table 1 presents a comparison between the actual and predicted coordinates of the sound source. It is evident that if the x or y values of the predicted sound source location differ from the actual values by more than 10 mm, or if the relative error exceeds 6.5%, it can be determined that the predicted sound source is not in the correct grid area. The incorrectly predicted grids were 2, 4, 14, and 17. Grids 2, 4, and 14 were incorrectly predicted to adjacent grids along the x-direction due to substantial deviation in the x-coordinate, while grid 17 was incorrectly predicted to an adjacent grid along the y-direction due to a large deviation in the y-coordinate (Figure 8 and Table 1). Comparing the incorrect predictions with the locations of the acoustic emission sensors in Figure 1 indicated that the incorrect sound source grids were all located far from the sensors. This indicated that the distance between the sound source and the sensors affected the localization accuracy. Using the SVR-based sound source

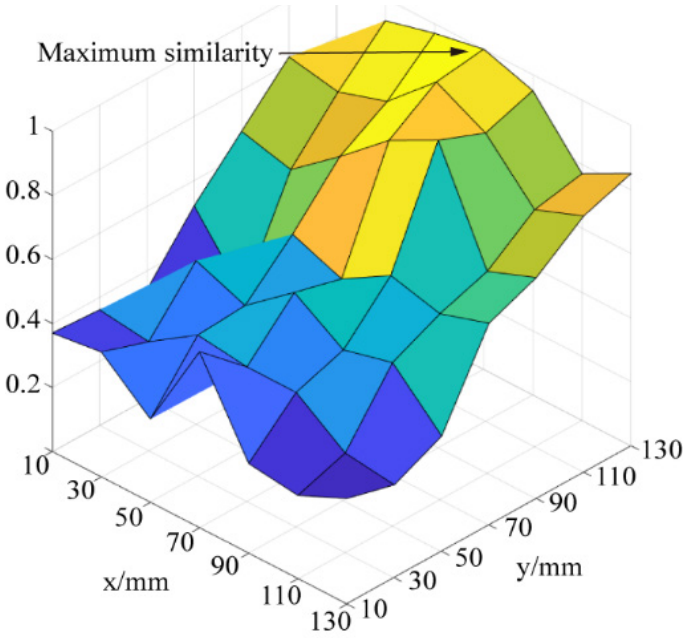

Figure 6. Similarity of feature vectors between the sample point signals and each point signal at coordinates (70mm, 130mm).

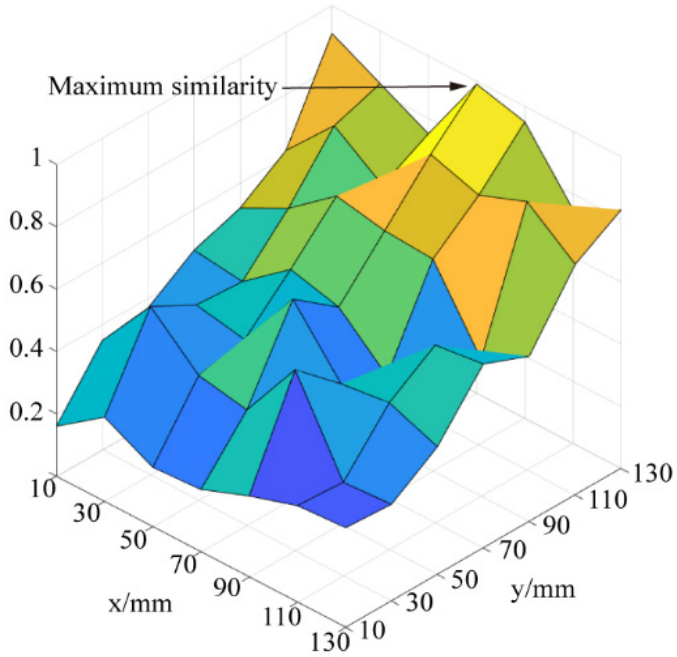

Figure 7. Similarity of feature vectors between the sample point signal and each test point signal at coordinates (70mm, 130mm).

Table 1. Comparison between actual sound source location and predicted values.

Actual Grid	Actual value x_0 /mm	Actual value y_0/ mm	Projected value x/mm	Predicted value y/mm	Absolute error/mm	Relative error/%	Prediction grids
1	10	10	16.3	5.7	7.63	3.85	1
2	30	10	18.5	16.6	13.26	6.70	1
3	50	10	47.2	12.9	4.03	2.04	3
4	70	10	83.8	8.2	13.92	7.03	5
5	90	10	85.0	16.0	7.81	3.94	5
6	110	10	114.2	14.3	6.01	3.04	6
7	130	10	137.3	16.1	9.51	4.80	7
8	10	30	7.0	22.8	7.80	3.94	8
9	30	30	22.8	38.7	11.29	5.70	9
10	50	30	54.7	28.2	5.03	2.54	10
11	70	30	77.8	23.7	10.03	5.06	11
12	90	30	93.3	23.0	7.74	3.91	12
13	110	30	114.1	35.1	6.54	3.31	13
14	130	30	117.6	24.6	13.52	6.83	13
15	10	50	17.8	52.6	8.22	4.15	15
16	30	50	23.4	44.5	8.59	4.34	16
17	50	50	57.9	62.8	15.04	7.60	24
18	70	50	64.1	51.6	6.11	3.09	18
19	90	50	95.8	52.9	6.48	3.28	19
20	110	50	101.7	55.2	9.79	4.95	20
21	130	50	133.5	53.1	4.68	2.36	21
22	10	70	6.2	66.6	5.10	2.58	22
23	30	70	27.3	71.7	3.19	1.61	23
24	50	70	55.6	76.1	8.28	4.18	24
25	70	70	62.1	71.7	8.08	4.08	25
26	90	70	92.6	64.4	6.17	3.12	26
27	110	70	112.6	68.1	3.22	1.63	27
28	130	70	137.7	61.5	11.47	5.79	28
29	10	90	2.0	81.8	11.46	5.79	29
30	30	90	26.7	82.5	8.19	4.14	30
31	50	90	41.9	91.4	8.22	4.15	31
32	70	90	66.8	96.2	6.98	3.52	32
33	90	90	92.9	87.7	3.70	1.87	33
34	110	90	118.4	85.1	9.72	4.91	34
35	130	90	132.9	93.0	4.17	2.11	35
36	10	110	14.4	117.8	8.96	4.52	36
37	30	110	33.5	112.5	4.30	2.17	37
38	50	110	46.8	106.3	4.89	2.47	38
39	70	110	76.5	103.4	9.26	4.68	39
40	90	110	84.0	113.1	6.75	3.41	40
41	110	110	105.7	112.3	4.88	2.46	41
42	130	110	124.6	114.4	6.97	3.52	42
43	10	130	12.9	124.3	6.40	3.23	43
44	30	130	32.5	128.2	3.08	1.56	44
45	50	130	44.9	135.6	7.57	3.83	45
46	70	130	63.6	127.9	6.74	3.40	46
47	90	130	92.9	128.1	3.47	1.75	47
48	110	130	113.3	136.7	7.47	3.77	48
49	130	130	124.0	128.4	6.21	3.14	49

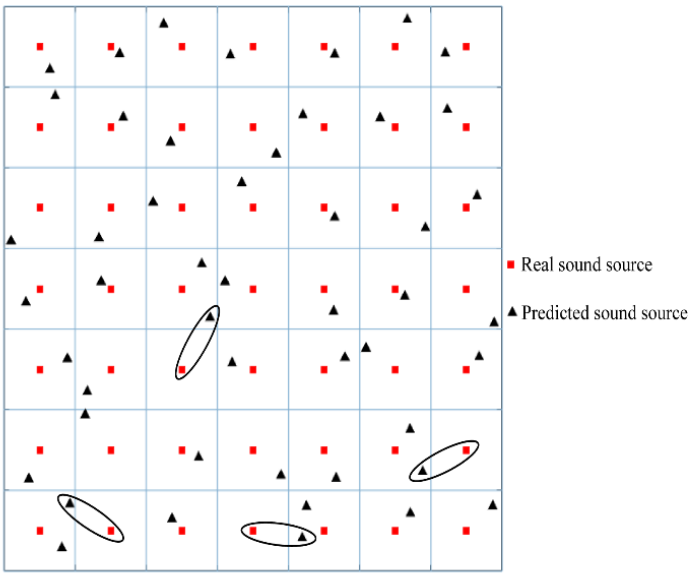

43	44	45	46	47	48	49
36	37	38	39	40	41	42
29	30	31	32	33	34	35
22	23	24	25	26	27	28
15	16	24	18	19	20	21
8	9	10	11	12	13	13
1	1	3	5	5	6	7

Figure 8. Prediction results of sound source location (a) Prediction of sound source location coordinates (b) Prediction of sound source location grid area.

localization method proposed in this study, the localization accuracy was 91.84%, demonstrating that this method achieved high accuracy. Additionally, based on previous research by Kim and Lee (2014), it can be speculated that further increasing the grid resolution, i.e., making the grid divisions finer, will lead to higher localization accuracy.

Conclusion

The acoustic emission acquisition system used to carry out the fir board pencil-lead break test showed that the closer the location of the acoustic emission source, the higher the similarity of the amplitude-frequency characteristics of the signals collected, and the farther the location of the source, the lower the similarity of the amplitude-frequency characteristics of the signals collected. After the signal noise reduction process, the energy feature vector was obtained by 9-layer WPD based on the db5 wavelet, and the first 8-dimensional feature vector was obtained by PCA to do the normalization process. The model of the SVR was constructed, and then the localization calculation was completed according to the SVR model. The average absolute error of the method was 7.51 mm, the average relative error was 3.79%, and the localization accuracy rate was 91.84%, which was obtained through the experiments of lead breakage localization of 140 mm × 140 mm fir boards. The research results show that the grid localization method of acoustic emission source based on SVR is feasible.

Acknowledgements

This work was supported by the “Beijing Natural Science Foundation Project (2182045)”.

References

Aicher S, Hofflin L, Dill-Langer G (2001). Damage evolution and acoustic emission of wood at tension perpendicular to fiber. Holz Roh Werkst 59(1-2):104–116. https://doi.org/10.1007/s001070050482

Ai M, Zhou X, Gao G, Gao S, Du X (2024). Falling damage behavior analysis and degree prediction for wooden pallet based on piezoelectric effect and acoustic emission. Eur J Wood Wood Prod 82(4):1227–1239. https://doi.org/10.1007/s00107-024-02064-4

Boccacci G, Frasca F, Bertolin C, Siani AM (2022). Influencing factors in acoustic emission detection: A literature review focusing on grain angle and high/low tree ring density of Scots pine. Appl Sci 12(2):859. https://doi.org/10.3390/app12020859

Bucur V (2023). A review on acoustics of wood as a tool for quality assessment. Forests 14(8):1545–1567. https://doi.org/10.1007/978-3-662-70209-3_13

Cruz C, Gaju M, Gallego A, Rescalvo F, Suarez E (2022). Non-destructive multi-feature analysis of a historic wooden floor. Buildings 12(12):2193. https://doi.org/10.3390/buildings12122193

Dinçkal C (2011). Analysis of elastic anisotropy of wood material for engineering applications. J Innov Res Eng Sci 2(2):67–80. https://doi.org/10.4314/ijest.v3i4.68553

Ebrahimkhanlou A, Salamone S (2018). Single-sensor acoustic emission source localization in plate-like structures using deep learning. Aerospace 5(2):50. https://doi.org/10.3390/aerospace5020050

Guo F, Zhang P, Zhang D, Han X, Fei Q (2017). Low speed impact localization of fiber Bragg grating based on wavelet packet energy feature vectors. Shock Vib 36:184–189. doi:10.13465/j.cnki.jvs.2017.08.029

Han Y, Chun Q, Wang H (2022). Quantitative safety evaluation of ancient Chinese timber arch lounge bridges. J Wood Sci 68(1):4–18. https://doi.org/10.1186/s10086-022-02011-y

He X, Zhu X (2024). Two-dimensional acoustic emission source localization on layered engineered wood by machine learning: a case study of laminated veneer lumber plate structure. Struct Health Monit 23(4):2423–2442. https://doi.org/10.1177/14759217231202544

Ji M, Zhang W, Diao X, Wang G, Miao H (2023). Intelligent automation manufacturing for Betula solid timber based on machine vision detection and optimization grading system applied to building materials. Forests 14(7):1510–1536. https://doi.org/10.3390/f14071510

Kim K, Lee Y (2014). Acoustic emission source localization in plate-like structures using least-squares support vector machines with delta t feature. J Mech Sci Tech 28:3013–3020. https://doi.org/10.1007/s12206-014-0707-0

Kundu T, Das S, Jata K (2007). Point of impact prediction in isotropic and anisotropic plates from the acoustic emission data. J Acoust Soc Am 122(4):2057–2066. https://doi.org/10.1121/1.2775322

Lamy F, Takarli M, Angellier N, Dubois F, Pop O (2015). Acoustic emission technique for fracture analysis in wood materials. Int J Fract 192:57–70. https://doi.org/10.1007/s10704-014-9985-x

Li X, Deng T, Wang M, Ju S, Li X, Li M (2020). Improvement of linear localization algorithm for wood acoustic emission sources based on wavelet and correlation analysis. J For Eng 5 (3):138–143. doi:10.13360/j.issn.2096-1359.201907045

Li Y, Yu SS, Dai L, Luo TF, Li M (2018). Acoustic emission signal source localization on plywood surface with cross-correlation method. J Wood Sci 64:78–84. https://doi.org/10.1007/s10086-017-1672-x

López G, Vallelado-Cordobes P, Gomez-Royuela J, Basterra L (2023). Diagnosis and assessment of a historic timber structure in La Casa del Corregidor, using non-destructive techniques. Case Stud Constr Mater 19:e02311. https://doi.org/10.1016/j.cscm.2023.e02311

Nocetti M, Mannucci M, Brunetti M (2023). Automatic assessment of insect degradation depth in structural solid wood elements by drilling resistance measurements. Constr Build Mater 366:130273. https://doi.org/10.1016/j.conbuildmat.2022.130273

Park C, Kim J, Jun S, Kim C (2012). Localizations and force reconstruction of low-velocity impact in a composite panel using optical fiber sensors. Adv Compos Mater 21(5-6):357–369. https://doi.org/10.1080/09243046.2012.736346

Pan X, Li M, Hu Q (2024). Study on acoustic emission parameter characteristics of damage in Chinese fir components with T-shaped and L-shaped cracks [J]. J Forest Industry 61(10):17–23. doi:10.19531/j.issn1001-5299.202410004

Qin G, Li M, Fang S, Deng T, Huang C, Mao F, Zhao Y, Xu N (2024). Study of a grid-based regional localization method for damage sources during three-point bending tests of wood. Constr Build Mater 419:135348. https://doi.org/10.1016/j.conbuildmat.2024.135348

Rescalvo FJ, Valverde-Palacios I, Suarez E, Roldan A, Gallego A (2018). Monitoring of carbon fiber-reinforced old timber beams via strain and multiresonant acoustic emission sensors. Sensors 18(4):1224. https://doi.org/10.3390/s18041224

Shrestha P, Kim J, Park Y, Kim C (2015). Impact localization on composite wing using 1D array FBG sensor and RMS/correlation based reference database algorithm. Compos Struct 125:159-169. https://doi.org/10.1016/j.compstruct.2015.01.029

Su H, Ou B, Tong J, Hu J, Wen Z (2012). Pattern recognition method for the source location of acoustic emission generated during the damage of hydraulic concrete. Strain 48(6):482-490.https://doi.org/10.1111/j.1475-1305.2012.00845.x

Xu N, Li M, Fang S, Huang C, Chen C, Zhao Y, Mao F, Deng T, Wang Y (2023). Research on the detection of the hole in wood based on acoustic emission frequency sweeping. Constr Build Mater 400:132761. https://doi.org/10.1016/j.conbuildmat.2023.132761

Xu P, Guan C, Zhang H, Li G, Zhao D, Ross RJ, Shen Y (2021). Application of nondestructive testing technologies in preserving historic trees and ancient timber structures in China. Forests 12(3):318. https://doi.org/10.3390/f12030318

Yin S, Xiao H, Cui Z, Kundu T (2021). Rapid localization of acoustic source using sensor clusters in 3D homogeneous and heterogeneous structures. Struct Health Monit 20(3):1145-1155. https://doi.org/10.1177/1475921720945195

Zhao X, Jiao L, Zhao J, Zhao D (2017). Acoustic emission attenuation characteristics and source localization during bending failure of mortise and tenon structures. J Beijing For Univ 39:107–111. doi:10.13332/j.1000-1522.20160150

Zhou W, Pan ZB, Wang J, Qiao S, Ma LH, Liu J, Ren XY, Liang YZ (2023). Review on acoustic emission source location, damage recognition and lifetime prediction of fiber-reinforced composites. J Mater Sci 58(2):583-607. https://doi.org/10.1007/s10853-022-08063-1